

OBSERVATION OF THE SURFACE CIRCULATION OF THE MEDITERRANEAN SEA FROM SPACE

Svetlana Karimova

*University of Liege, Department of Astrophysics, Geophysics, and Oceanography,
GeoHydrodynamic and Environmental Research Unit,
Allée du 6 Août, 17, Bât. B5, 4000 Liège, Belgium,
Email: svetlana.karimova@ulg.ac.be*

ABSTRACT

In the present work mesoscale eddies of the Western Mediterranean are being investigated by means of thermal imagery and altimetry data. Comparison of 1489 anticyclonic and 782 cyclonic eddy manifestations found in sea surface temperature (SST) imagery on an analysis of a 3-year-long dataset (covering the period from 2011 to 2013) with corresponding sea level anomaly (SLA) fields showed that only anticyclonic eddies exceeding ca. 70 km in diameter can be more or less sustainably manifested in the fields of SLA and its derivatives (such as relative vorticity). Detection of cyclonic eddies on base of SLA data, presumably due to the small spatial and temporal scales of such eddies and their non-geostrophic nature, is problematic.

1. INTRODUCTION

In coastal regions and in the open ocean, mesoscale vortical structures play a crucial role in determining statistical properties of the turbulence field. In addition, these features can significantly affect the water transport properties in the water bodies and thus modulate the dynamics of their ecosystems.

The western Mediterranean Sea is an area of intensive mesoscale eddy activity. The biggest, most persistent, and most studied eddies of the basin are being observed in the Alboran Sea (so called Alboran Eddies). These are one or two anticyclonic gyres with a diameter of about 100 km, which originate due to the inflow of Atlantic water through the Strait of Gibraltar [1-2].

Large gyres are frequently observed in the Algerian Basin as well. In that area anticyclonic eddies with a diameter up to 200 km come into being as a result of instability of the Algerian Current. Such vortices propagate eastward along the Algerian slope [3]. In the vicinity of the Channel of Sardinia, they can detach from the Algerian slope and propagate along the Sardinian one [3-4].

At times satellite thermal imagery reveal huge and driftless anticyclonic eddies occupying most of the Algerian basin [5]. The presence of these big eddies has a large impact on the surface and intermediate circulation in this area [1, 6].

A generalized statistical analysis of mesoscale eddies seen in thermal imagery of the Mediterranean Sea has not been performed yet. On base of satellite altimetry, such an analysis was provided by [7], which showed that among the vortices with high values of amplitude, energy, and size anticyclonic eddies were prevailing while in general approximately similar numbers of cyclonic and anticyclonic vortices were discovered.

In the present study, we scrutinize in greater detail manifestation of mesoscale eddies in the satellite-derived fields of SLA and SST using 3-year long daily datasets of those parameters. The need in such a comparison is explained by the significant discrepancies in the results gained using SST and SLA data. Thus, from an analysis of satellite imagery it is known that in the marginal and inner seas strong anticyclonic dominance is usually being observed among mesoscale eddies [8-10]. At the same time, the SLA-based methods usually reveal similar characteristics for cyclonic and anticyclonic eddies [7, 11].

As a region of interest (ROI) the western Western Mediterranean (approx. up to 9° W) is being used, which is having especially prominent mesoscale eddy activity and for which the most suitable for the current study datasets were obtained.

2. DATA USED

Used in the present study daily SST images of ROI have been obtained at the SOCIB (Balearic Islands Coastal Observing and Forecasting System) data portal (<http://www.socib.es/>). Pixel size of the images is about 1 km. The dataset analysed covers the period from 2011 to 2013. An example of SST field for ROI obtained on 01.09.2014 is shown in Fig. 1. A series of big anticyclonic and smaller cyclonic eddies can be clearly discerned in the southern part of the basin.

The second product used, namely daily SLA fields for the entire Mediterranean Sea for the same years as the SST imagery, have been provided by the Collecte Localisation Satellites Group (CLS), Toulouse, France, and downloaded at the Copernicus Marine Environment Monitoring Service (<http://marine.copernicus.eu/>). The product is based on multi-altimeter SLA computed using a twenty-year mean sea surface height.

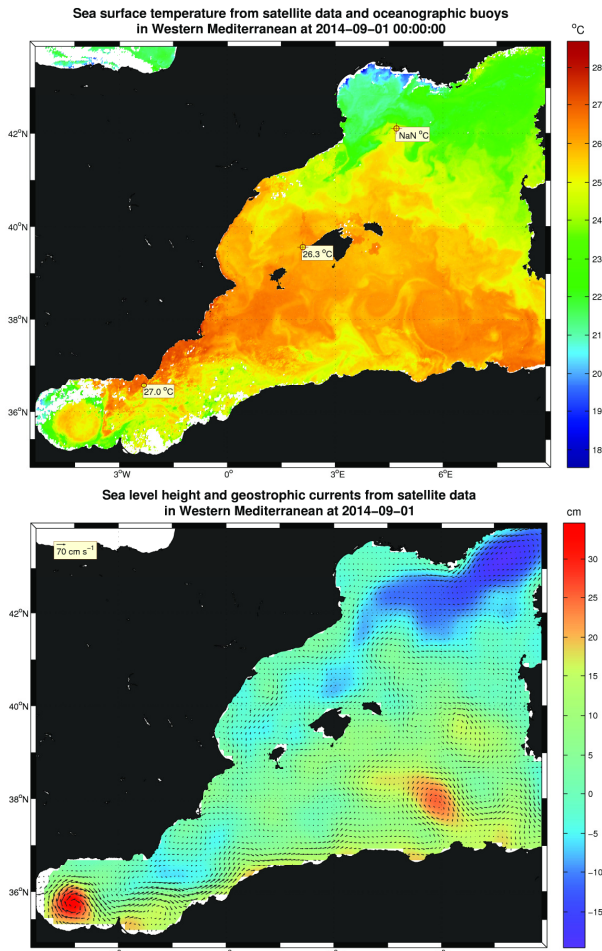


Figure 1. Examples of SST (upper panel) and SLA (lower panel) fields for the region of interest.

All altimeter missions have been homogenized with respect to a reference one, which is Jason-2. The data have been cross validated, filtered from residual noise and small scale signals, and sub-sampled. Finally gridded SLA fields have been obtained via an optimal interpolation algorithm. Grid resolution of the product is 0.125° . An example of a SLA field corresponding to the same date as the SST field is also shown in Fig. 1. In general, big anticyclonic eddies visible in the SST field (upper panel) refer to the greatest positive values of SLA (lower panel).

3. PROCESSION OF THE SST IMAGERY

SST imagery mentioned in the previous subsection have been visually scrutinized and visible eddy manifestations have been fixed manually. As eddy manifestations circular or elliptically shaped patches with a tendency to spirality have been considered. For every manifestation found the coordinates of its centre as well as spatial scale and sign of vorticity have been defined. Due to long lifetimes of some eddies, their presence in the imagery could have been reported several times.

4. PROCESSION OF THE SLA FIELDS

In order to check whether eddy manifestations found in the SST fields had some signal noticeable in the corresponding fields of SLA and its derivatives, the following procedure has been performed. Following earlier published works on application of satellite altimetry data for mesoscale eddy detection, some additional dynamical fields were calculated based on the SLA data. Among them there are:

- zonal and meridional components of the surface currents field derived using the geostrophic approximation [7]; knowing these two components of the geostrophic currents is necessary for calculation of the parameters mentioned below;
- relative vorticity usually being used for calculating the parameters following below rather than for a direct eddy detection;
- Q-parameter, Q , representing the second invariant of the velocity gradient tensor and characterizing the local balance between shear strain rate and vorticity magnitude [12], since at positive Q the rotation dominates over the deformation, an eddy is supposed to exist in regions where Q is positive and relatively large; this parameter has been used for eddy detection in the Algerian Basin of the Western Mediterranean [12], in the main upwelling systems of the World Ocean [13], and in the California Current System [14];
- Okubo-Weiss parameter, W , widely used in the studies of two-dimensional turbulence; similar to the Q-parameter, Okubo-Weiss parameter provides information about the relative dominance of strain and vorticity; since vortices are regarded as single connected regions of concentrated vorticity in which there is a dominance of vorticity over strain, the Okubo-Weiss parameter offers a basis for a vortex identification criterion as a region with negative values of W [7]; this parameter is frequently used for eddy detection on base of satellite altimetry and numerical modelling data [7, 15-17].

On calculating the fields of the parameters listed above the nearest to the eddy centres values of these parameters for the same date have been retrieved. After that a regional algorithm for detection of possible eddy manifestation in the fields of SLA has been proposed and applied. The results have been compared with those provided by the SST imagery.

5. EDDIES FOUND IN THE SST IMAGERY

In the SST imagery of the Western Mediterranean obtained in 2011-2013 a total of 1489 anticyclonic and 782 cyclonic eddy manifestations were detected. Centres of anticyclonic and cyclonic eddies found are shown in Fig. 2.

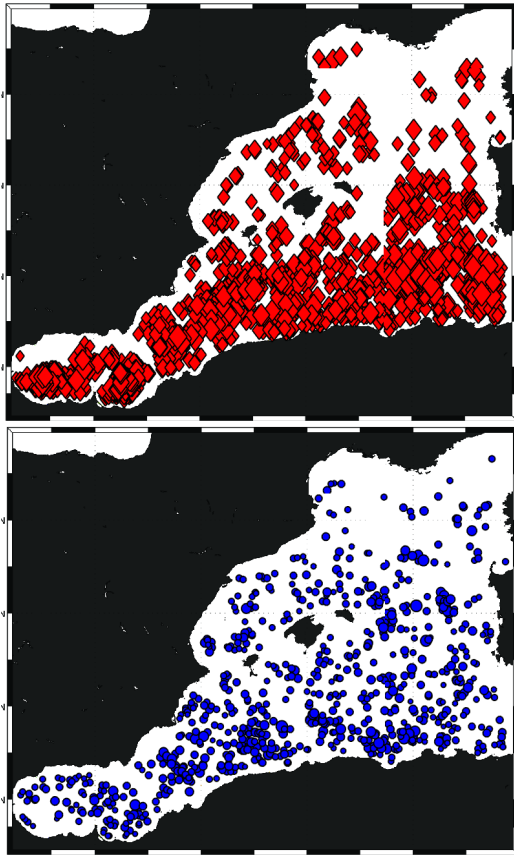


Figure 2. Spatial distribution of anticyclonic (top panel) and cyclonic (low panel) eddy manifestations.

Anticyclonic eddies were especially frequently detected in the area off the southern coast of the basin (Fig. 2, upper panel). Cyclonic eddies found were distributed more evenly in space. Similar to anticyclonic eddies, the number of manifestations found is decreasing from south to north (Fig. 2, lower panel).

Normalized distribution of eddy diameters is given in Fig. 3.

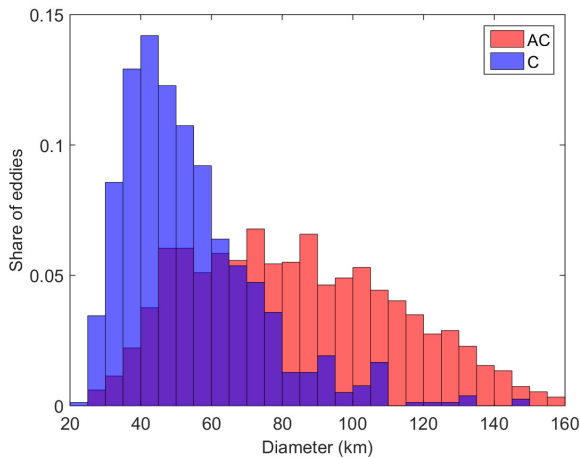


Figure 3. Normalized distribution of diameters of anticyclonic (AC) and cyclonic (C) eddies.

6. SLA VALUES IN THE VICINITY OF EDDIES

In order to check whether eddies found in SST had a signal in SLA fields as well, for every eddy manifestation the closest (in space and time) to its centre values of h , ω , Q , and W have been found. In Fig. 4 such values for h , ω , and Q are shown plotted versus eddy diameter values.

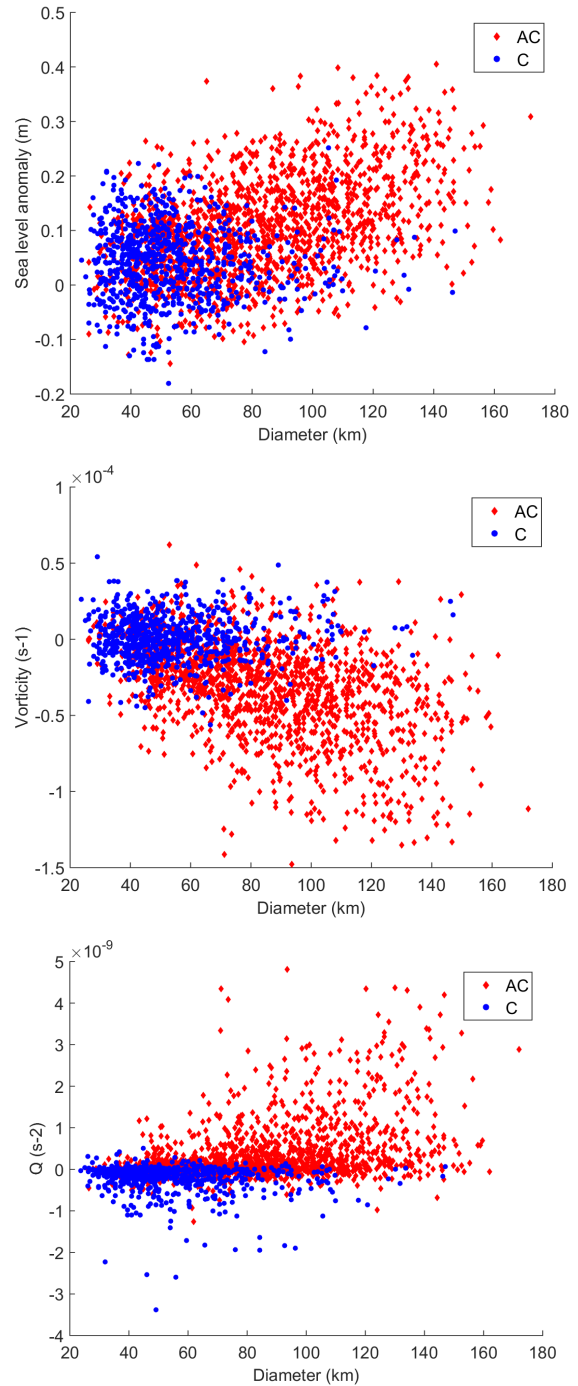


Figure 4. Values of SLA (upper panel), relative vorticity (middle panel), and Q -parameter (lower panel) corresponding to eddies found in SST plotted versus the values of eddy diameters.

For anticyclonic eddies (Fig. 4, upper panel), it is notable that most eddies (more precisely 88.2%) corresponded to the positive values of SLA. Moreover, there is a regression (supposedly linear) between an eddy size and the corresponding SLA magnitude (Fig. 4, upper panel), meaning that the bigger an eddy spatial scale, the bigger the corresponding SLA value.

The same plot demonstrates that the SLA values corresponding to cyclonic eddies are different from what could be expected. Most of the eddy manifestations (73.3 %) referred to positive values of SLA (Fig. 4, upper panel), even though cyclonic eddies were expected to have a negative SLA value in their centres. Variance of SLA values corresponding to cyclonic eddies is smaller than that of values corresponding to anticyclonic eddies. Thus, the latter are mostly varying within -0.1 - +0.2 m, while the former are reaching 0.4 m (Fig. 4, upper panel).

A similar plot for relative vorticity is given in Fig. 4, middle panel. Again, as it was expected, anticyclonic eddies tend to have negative values of relative vorticity in the vicinity of their centres. In total about 87.3% of anticyclonic eddies corresponded to negative values of relative vorticity. The minimum value of relative vorticity in the vicinity of anticyclonic eddies reached about $-1.5 \times 10^{-4} \text{ s}^{-1}$.

Relative vorticity values corresponding to cyclonic eddies are almost symmetrically located on both sides of the plot with 52.0 % of the values being above the axis (Fig. 4, middle panel). Thus, as far as cyclonic eddies are concerned, relative vorticity seems slightly more suitable for eddy detection than SLA.

Distribution of the Q-parameter values in the vicinity of eddies is shown in Fig. 4, lower panel. In this case both cyclonic and anticyclonic eddies tended to have absolute values of Q close to zero. Only some (mostly big) anticyclonic eddies corresponded to quite large positive values of Q (Fig. 4, lower panel). Positive Q-values had 70.4% of anticyclonic eddies and 17.6% of cyclonic ones.

Similar situation was observed with the Okubo-Weiss parameter (not shown here). Almost none of cyclonic eddies demonstrated particularly large negative values of W. The percentage of positive and negative W-values for anticyclonic eddies was exactly the opposite of those of Q-values. Among cyclonic eddies 32.1% had negative W-values.

For a conclusion, Table 1 shows the percentage of anticyclonic and cyclonic eddies having the corresponding values of H, ω , Q, and W of an 'expected' sign. On analysis of Table 1, we can conclude that for anticyclonic eddies all four parameters performed quite good. For cyclonic eddies, such performance of the parameters in representing an 'expected' sign was much worth.

Table 1. Percentage of eddies corresponding to the values of an 'expected' sign (%).

Parameter	AC eddies	C eddies
H	88.2	26.7
ω	87.3	52.0
Q	70.4	17.6
W	70.4	32.1

7. DETECTING AND TRACKING POSSIBLE EDDY MANIFESTATIONS IN SLA

As it was concluded in the previous section, among the four parameters considered anticyclonic eddies had the greatest signal in the fields of SLA and relative vorticity. For cyclonic eddies, such a parameter was relative vorticity. Based on that, in the present subsection SLA and relative vorticity fields will be used for an automated detection of possible eddy manifestations.

Since using certain thresholds (different from zero) would automatically exclude a possibility of detecting some significant numbers of eddies (Fig. 4, upper and middle panels), using a thresholdless approach would be preferable. Similar to [18-20], in the present work a closed-contour, or winding-angle, method has been applied.

First, for all SLA and relative vorticity fields available for the period of the present study contour plots have been provided. The contours had 0.01 m and 10^{-5} s^{-1} intervals for SLA and relative vorticity, respectively. As a possible eddy manifestation in these contour plots an area limited by a closed (or almost closed – in the near-coastal area) contour with a local extremum of a required sign was considered.

After that, since among the contours chosen there still could be multiple 'false alarms', a procedure of contour tracking has been performed. For that, for every contour chosen it was checked whether there was another contour located nearby at a present or adjacent date. If there were at least two contours found at almost same place, these contours were considered as a possible eddy manifestation. Since the presence of a SLA contour is usually a stronger condition than that of a relative vorticity contour, at least one SLA contour among all contours denoting an eddy manifestation was additionally required to be found.

It was noticed that the region of interest is much denser populated with the contours (not shown) than it was previously with eddy manifestations found in SST imagery (Figs. 2-3). Locations of the most long-lived series of contours (with a lifetime exceeding 6 days) for anticyclonic and cyclonic eddies can be seen in Fig. 5. The marker size is representing the lifetime of an eddy. It is notable that the long-lived series of contours mostly corresponded to (presumably big) eddies attributed to the Atlantic water flow (Fig. 5).

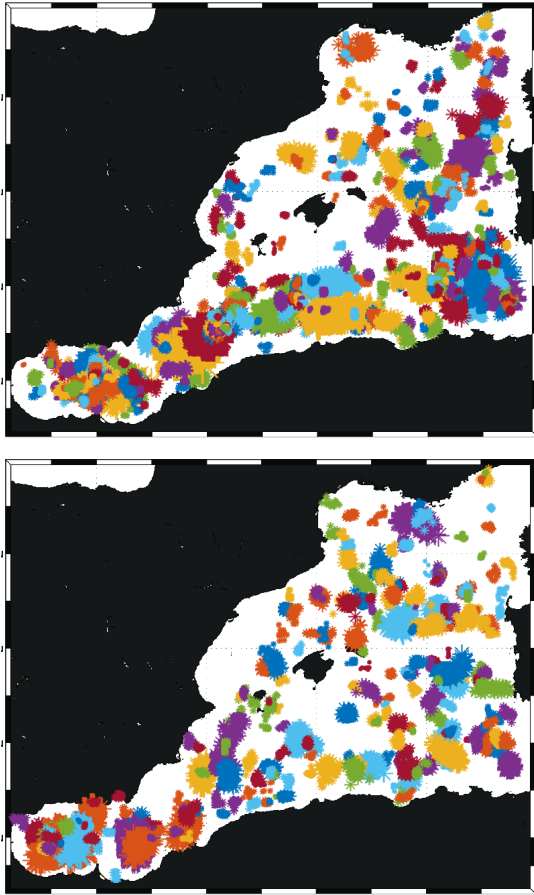


Figure 5. Locations of the most long-lived series of contours corresponding to anticyclonic (top panel) and cyclonic (low panel) eddies. Contours are referring to the same eddy are shown with the same colour. Marker size is proportional to the lifetime of a series.

After that a check was performed whether the contours chosen corresponded to eddy manifestations found in SST. In case a contour did the extreme value within such a contour was noted. A distribution of such derived extremum values was compared to that of the extremum values of all contours chosen. Such normalized distributions of the extremum values of SLA and relative vorticity are presented in Figs. 6 and 7.

As it was expected, in general the contours corresponding to anticyclonic eddies found in SST imagery tend to have higher values of SLA compared to all contours. Thus, about 90% of the contours corresponding to an anticyclonic eddy in SST imagery had values of SLA exceeding 0.8 m.

Contours corresponding to cyclonic eddies found in SST, in contrary, referred to small and moderate absolute values of SLA (Fig. 6) not exceeding 0.13 m. Such distribution of the extremum SLA values confirms mentioned earlier impossibility of introducing thresholds for an automated extraction of possible cyclonic eddy manifestations in the fields of SLA.

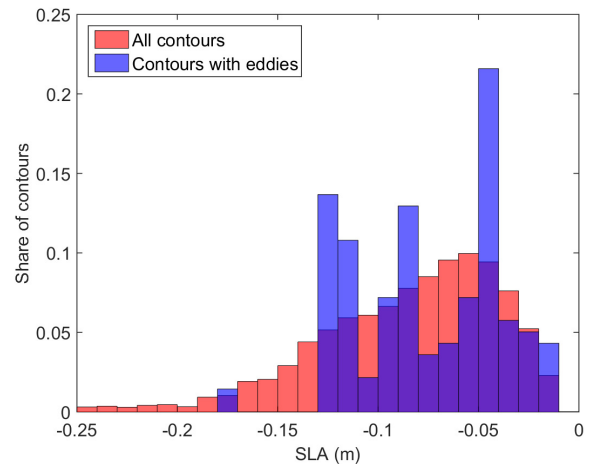
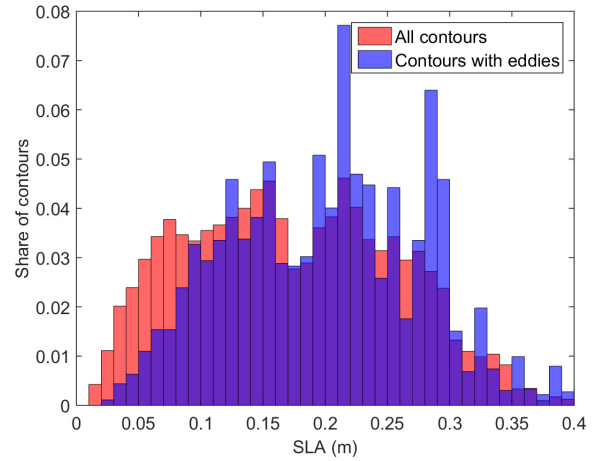


Figure 6. Normalized distributions of SLA extremum values within all contours chosen and within those corresponding to eddies found in SST. Upper panel: anticyclonic eddies, lower cyclonic eddies.

Similar graphs showing the attributed to the contours extremum values of relative vorticity are given in Fig. 7. This time the extremum values corresponding to anticyclonic eddies again corresponded to higher absolute values of relative vorticity; values corresponding to cyclonic eddies in SST imagery were greater than those of all contours as well (Fig. 7, lower panel). Thus, once again it is noticeable that for cyclonic eddy detection relative vorticity fields performed better than those of SLA.

In general, more than 90% of the contours corresponding to anticyclonic and 75% of those corresponding to cyclonic eddies had the absolute values exceeding $6.0 \cdot 10^{-5} \text{ s}^{-1}$. The values $-7.0 \cdot 10^{-5} \text{ s}^{-1}$ and $6.0 \cdot 10^{-5} \text{ s}^{-1}$ could be used as a threshold for an automated detection of possible anticyclonic and cyclonic eddy manifestations, respectively, in the fields of relative vorticity. Since the pairs of distributions considered are quite close, one has to notice, that at any threshold chosen, there is still a high chance of encountering a 'false alarm' (Figs. 7-8).

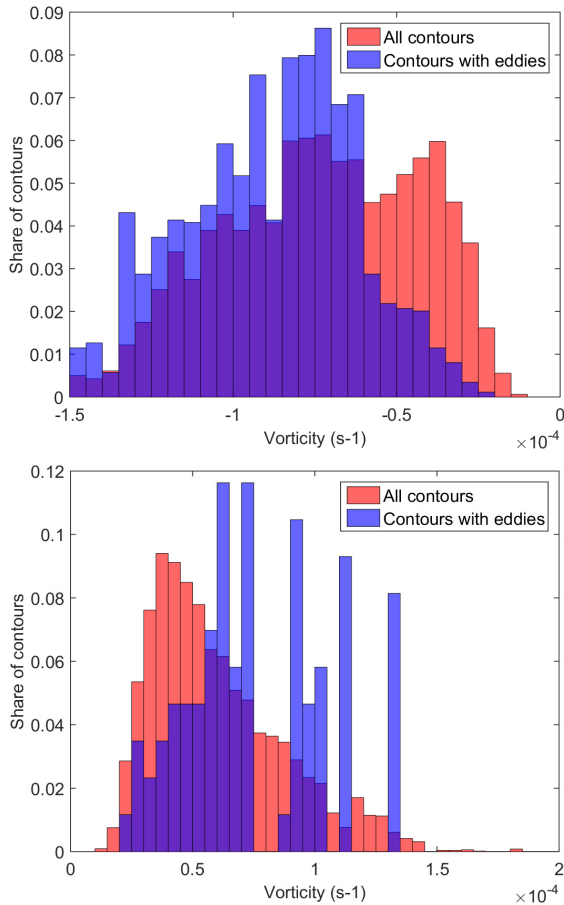


Figure 7. Normalized distributions of the relative vorticity extremum values within all contours chosen and within those corresponding to eddies found in SST. Upper panel: anticyclonic eddies, lower cyclonic eddies.

8. COMPARISON WITH EDDIES IN SST

As a final step, correspondence of eddies found in SST imagery to SLA and relative vorticity contours was assessed. In general, about 36.7% of anticyclonic eddies and 9.2% of cyclonic ones had some corresponding closed contours in SLA and relative vorticity fields.

Spatial distribution of eddies that had a corresponding contour is shown in Fig. 8. In this figure, locations of eddies found in the SST imagery and confirmed by the contours are denoted with dark-red markers, while markers for eddies not corresponding to any contour are left grey.

It is notable that anticyclonic eddies attributed to the Atlantic water flow were manifested by the contours more frequently than eddies in other regions (Fig. 8, upper panel). Being quite large and long-living, these eddies have a greater chance to get manifested in a SLA field. Cyclonic eddies corresponded to the Atlantic water flow at less extent (Fig. 8, lower panel).

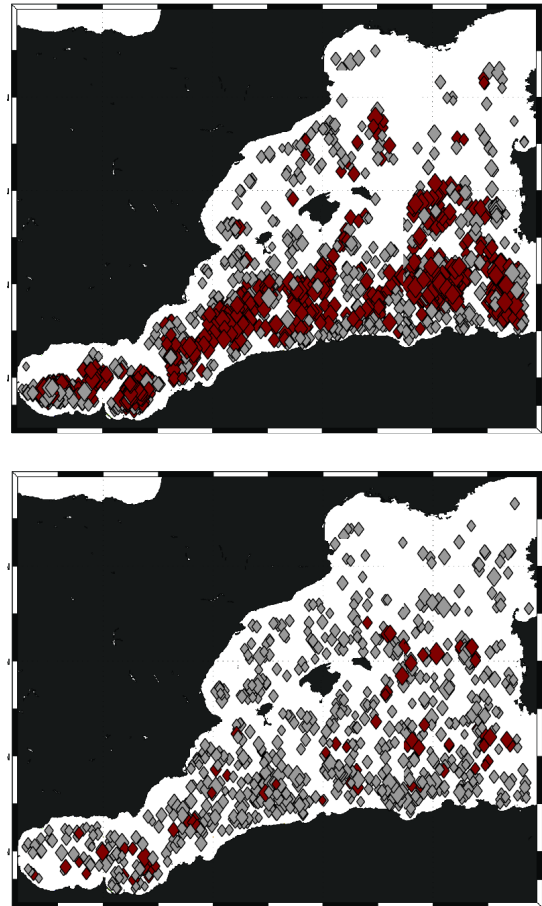


Figure 8. Locations of anticyclonic (upper panel) and cyclonic (lower panel) eddies found on analysis of SST imagery. Red markers denote eddies that had corresponding contours of SLA and relative vorticity, grey ones denote those that had not.

Finally, a distribution of eddy diameters corresponding to some contours was compared to the background distribution of eddy diameters. In Fig. 9 there are the absolute distributions of the numbers of eddies over different diameter values for anticyclonic and cyclonic eddies.

Fig. 9, upper panel, makes it obvious that manifestation of anticyclonic eddies by the SLA and relative vorticity contours significantly depends on eddy size. Thus, eddies smaller than 40 km in diameter were not seen in the contours at all, while eddies greater than 100 km corresponded to some contours at almost 100% (Fig. 9, upper panel).

For cyclonic eddies, such a tendency was much less persistent, and partly the distribution of diameter values of eddies corresponding to some contours followed the general distribution of diameters of cyclonic eddies detected in SST imagery (Fig. 9, lower panel).

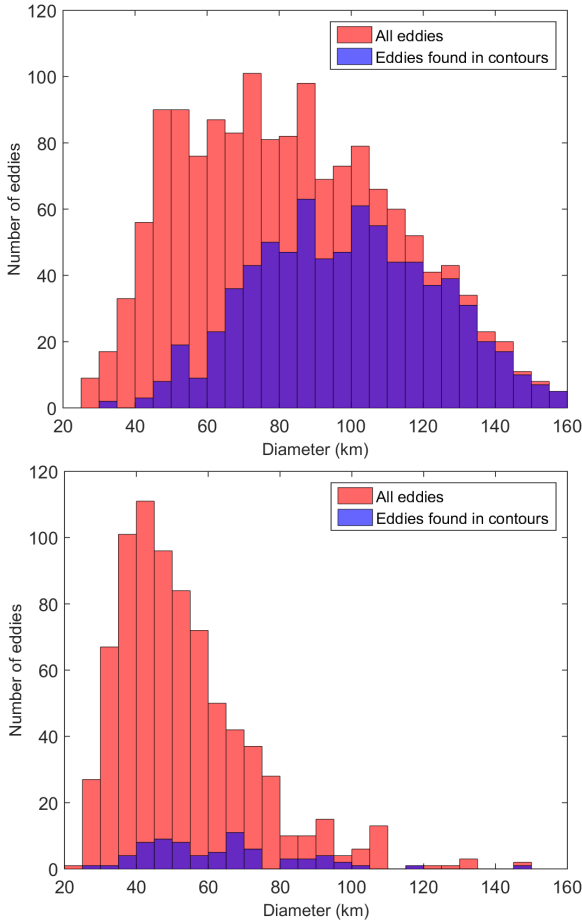


Figure 9. Absolute distributions of anticyclonic (upper panel) and cyclonic (lower panel) eddies over different spatial scales and of those having corresponding SLA and relative vorticity contours.

9. SUMMARY AND CONCLUSIONS

In the present study, a comprehensive comparison of mesoscale eddy manifestation in quasi-simultaneously obtained SST imagery and SLA fields has been performed for the first time.

Detection of eddies in the SST imagery revealed anticyclonic eddy dominance both in number and in size. A total of 1489 anticyclonic and 782 cyclonic eddy manifestations were found on an analysis of a 3-year-long dataset. Mean diameter of anticyclonic eddy manifestations was about 83.5 km, while that of cyclonic eddies about 53.6 km.

Retrieving some additional parameters (relative vorticity, Q-parameter, and Okubo-Weiss parameter) from the SLA fields showed that in general in the vicinity of centres of anticyclonic eddies these parameters had greater absolute values than in the vicinity of cyclonic eddies.

Among the four parameters being under consideration (SLA, relative vorticity, Q-parameter, and Okubo-Weiss parameter) the best ones for detecting anticyclonic

eddies were discovered to be SLA and relative vorticity. For cyclonic eddies such a parameter was relative vorticity.

A thresholdless closed-contour, or winding-angle, approach has been applied for detecting possible eddy manifestations in the fields of SLA and relative vorticity. If a contour corresponded to an eddy manifestation in SST imagery, the extremum value within such a contour was noted. About 90% of contours corresponding to an anticyclonic eddy in SST imagery had values of SLA exceeding 0.8 m. Contours corresponding to cyclonic eddies, in contrary, tended to have small and moderate absolute values of SLA. As for relative vorticity, more than 90% of contours corresponding to anticyclonic and 75% of those corresponding to cyclonic eddies had the absolute values exceeding $6.0 \cdot 10^{-5} \text{ s}^{-1}$.

A comparison of the locations of eddies found in SST with the contours retrieved from SLA and relative vorticity fields yielded that in general about 36.7% of anticyclonic eddies had corresponding contours in SLA and relative vorticity fields. Such percentage was different for eddies of different spatial scales. Thus, eddies smaller than 40 km in diameter did not correspond to any SLA or relative vorticity contours at all, while those bigger than 100 km corresponded to some of them at almost 100 %.

For cyclonic eddies, presumably due to their smaller spatial and temporal scales and non-geostrophic nature, the percentage of manifestations found both in SST and in the contours were only about 9.2 %. Unlike the case with anticyclonic eddies, a clear dependence of eddy representation in SLA and relative vorticity contours on eddy size was not observed and partly the distribution of diameter values of eddies corresponding to some contours followed the general distribution of diameters of cyclonic eddies detected in SST imagery.

On the analysis presented one can conclude that, despite being quite useful for a general study of mesoscale kinetic energy, satellite-derived SLA fields can be only of a limited use for providing mesoscale eddies statistics for the inner seas, since only the biggest anticyclonic eddies can be reliably detected in such fields.

Finally, we can conclude that at least for the inner seas closed contours in the fields of SLA and its derivatives are not synonymous with mesoscale eddies.

10. ACKNOWLEDGEMENTS

The SAR data were obtained under the grant of the European Space Agency # 14120 “Spiral eddy statistical analyses for the Mediterranean Sea using Envisat ASAR Imagery (SESAMeSEA)”.

This research was supported by the University of Liege and the EU in the context of the FP7-PEOPLE-COFUND-BelIPD project.

11. REFERENCES

1. Millot, C. (1987). Circulation in the Western Mediterranean Sea. *Oceanologica Acta*, **10**, 143–149.
2. Font, J., Rousseau, S., Shirasago, B., García-Górriz, E., & Haney, R.L. (2002). Mesoscale variability in the Alboran Sea: Synthetic aperture radar imaging of frontal eddies. *J. Geophys. Res.*, **107**(C6), 3059.
3. Puillat, I., Taupier-Letage, I., & Millot, C. (2002). Algerian eddies lifetime can near 3 years. *J. Marine Syst.*, **31**, 245–259.
4. Salas, J., Millot, C., Font, J., & García-Ladona, E. (2002). Analysis of mesoscale phenomena in the Algerian basin from drifting buoys and infrared images. *Deep-Sea Res., Part I*, **49**, 245–266.
5. Taupier-Letage, I. & Millot, C. (1988). Surface circulation in the Algerian basin during 1984. *Oceanologica Acta*, 79–85.
6. Isern-Fontanet, J., Font, J., Garcia-Ladona, E., Emelianov, M., Millot, C., & Taupier-Letage, I. (2004). Spatial structure of anticyclonic eddies in the Algerian basin (Mediterranean Sea) analyzed using the Okubo–Weiss parameter. *Deep-Sea Res.*, **51**, 3009–3028.
7. Isern-Fontanet, J., García-Ladona, E., & Font, J. (2006). Vortices of the Mediterranean Sea: An altimetric perspective. *J. Phys. Oceanogr.*, **36**, 87–103.
8. Zatsepin, A., Ginzburg, A., Kostianoy, A., Kremenetskiy, V., Krivosheya, V., Stanichny, S., & Poulain, P.-M. (2003). Observations of Black Sea mesoscale eddies and associated horizontal mixing. *J. Geophys. Res.*, **108**(C8), 3246, doi:10.19/2002JC001390.
9. Font, J., Isern-Fontanet, J., & Salas, J. (2004). Tracking a big anticyclonic eddy in the western Mediterranean Sea. *Scientia Marina*, **68**(3), 331–342.
10. Karimova, S. (2013). Non-stationary eddies in the Black Sea as seen by satellite infrared and visible imagery. *Int. J. Remote Sens.*, **34**, 8503.
11. Kubryakov, A.A. & Stanichny, S.V. (2015). Seasonal and interannual variability of the Black Sea eddies and its dependence on characteristics of the large-scale circulation. *Deep-Sea Res., Part I*, **97**, 80–91.
12. Isern-Fontanet, J., García-Ladona, E., & Font, J. (2003). Identification of marine eddies from altimetry. *J. Atmos. Oceanic Technol.*, **20**, 772–778.
13. Morrow, R., Birol, F., Griffin, D., & Sudre, J. (2004). Divergent pathways of cyclonic and anti-cyclonic ocean eddies. *Geophys. Res. Lett.*, **31**, L24311, doi:10.1029/2004GL020974.
14. Kurian, J., Colas, F., Capet, X., McWilliams, J.C., & Chelton, D.B. (2011). Eddy properties in the California Current System. *J. Geophys. Res.*, **116**, C08027, doi:10.1029/2010JC006895.
15. Chelton, D.B., Schlax, M.G., Samelson, R.M., & de Szoeke, R.A. (2007). Global observations of large oceanic eddies. *Geophys. Res. Lett.*, **34**, L15606, doi:10.1029/2007GL030812.
16. Souza, J.M.A.C., de Boyer Montegut, C., & Le Traon, P.Y. (2011). Comparison between three implementations of automatic identification algorithms for the quantification and characterization of mesoscale eddies in the South Atlantic Ocean. *Ocean Science*, **7**, 317–334.
17. Mill, G.N., da Costa, V.S., Lima, N.D., Gabioux, M., Guerra, L.A.A., & Paiva, A.M. (2015). Northward migration of Cape São Tomé Rings - Brazil. *Cont. Shelf Res.*, **106**, 27–37.
18. Chaigneau, A., Eldin, G., & Dewitte, B. (2009). Eddy activity in the four major upwelling systems from satellite altimetry (1992–2007). *Progr. Oceanogr.*, **83**, 117–123.
19. Chaigneau, A., Gizolme, A., & Grados, C. (2008). Mesoscale eddies off Peru in altimeter records: Identification algorithms and eddy spatio-temporal patterns. *Progr. Oceanogr.*, **79**, 106–119.
20. Chelton, D.B., Schlax, M.G., & Samelson, R.M. (2011). Global observations of nonlinear mesoscale eddies. *Progr. Oceanogr.*, **91**, 167–216.